Radiometric calibration of IR Fourier transform spectrometers: solution to a problem with the High-Resolution Interferometer Sounder

Henry E. Revercomb, H. Buijs, Hugh B. Howell, D. D. LaPorte, William L. Smith, and L. A. Sromovsky

A calibrated Fourier transform spectrometer, known as the High-Resolution Interferometer Sounder (HIS), has been flown on the NASA U-2 research aircraft to measure the infrared emission spectrum of the earth. The primary use—atmospheric temperature and humidity sounding—requires high radiometric precision and accuracy (of the order of 0.1 and 1°C, respectively). To meet these requirements, the HIS instrument performs inflight radiometric calibration, using observations of hot and cold blackbody reference sources as the basis for two-point calibrations at each wavenumber. Initially, laboratory tests revealed a calibration problem with brightness temperature errors as large as 15°C between 600 and 900 cm^{-1}. The symptom of the problem, which occurred in one of the three spectral bands of HIS, was a source-dependent phase response. Minor changes to the calibration equations completely eliminated the anomalous errors. The new analysis properly accounts for the situation in which the phase response for radiance from the instrument itself differs from that for radiance from an external source. The mechanism responsible for the dual phase response of the HIS instrument is identified as emission from the interferometer beam splitter.

I. Introduction

The capability of measuring absolute radiance with an infrared Fourier transform spectrometer is important to the High-Resolution Interferometer Sounder (HIS) program,[1,2] which is applying interferometry to measure the upwelling emission spectrum of the earth for retrieving the temperature, humidity, and other parameters of the atmosphere and surface. The primary objective of the HIS program is to improve significantly the vertical resolution of temperature and humidity profiles determined from satellite platforms by increasing the spectral resolution of observed radiances. The interferometer is a natural choice for the job. Interferometers have proved their merit in space with successful measurements of the emission spectra of planetary atmospheres, not only of the earth,[3,4] but also of Venus,[5] Mars,[6] Jupiter, Saturn and Uranus.[7] The multiplex and throughput advantages of the interferometer[8] make it possible to make radiometrically precise observations at a much higher spectral resolution than that of current filter radiometers (tens of cm^{-1}). To improve the vertical resolution in the troposphere and lower stratosphere by at least a factor of 2 over that of current temperature profiling radiometers (3–8 km), a resolving power ($\lambda/\Delta\lambda$) of ~1000 is needed in the spectral range from 3.7 to 17 μm. (The 15-μm CO_2 absorption band is the primary band for temperature sounding, the combined 4.3-μm CO_2 and 4.5-μm N_2O bands are used to enhance the temperature resolution in the lower troposphere, and the 6.7-μm H_2O absorption band gives humidity soundings.) High radiometric precision is required because radiometric noise and time-dependent and wavelength-dependent calibration errors are magnified in the inversion process to derive atmospheric parameters. To obtain temperature profiles with rms errors of <1°C from high-resolution measurements requires noise-equivalent-temperature errors and calibration reproducibilities of the order of 0.1°C and absolute errors of less than about 1°C.

Several important steps have been taken toward developing an improved temperature and humidity sounding satellite instrument. The feasibility of building an instrument to achieve the radiometric performance needed from a geosynchronous satellite plat-

H. Buijs is with BOMEM, Inc., 625 Marais, Ville de Vanier, Quebec G1M 2Y2, Canada; H. B. Howell is with NOAA/NESDIS Systems Design & Applications Branch, 1225 West Dayton Street, Madison, Wisconsin 53706; D. D. LaPorte is with Santa Barbara Research Center, 75 Coromar Drive, Goleta, California 93117; and the other authors are with University of Wisconsin, Space Science & Engineering Center, 1225 West Dayton Street, Madison, Wisconsin 53706.

Received 19 December 1987.

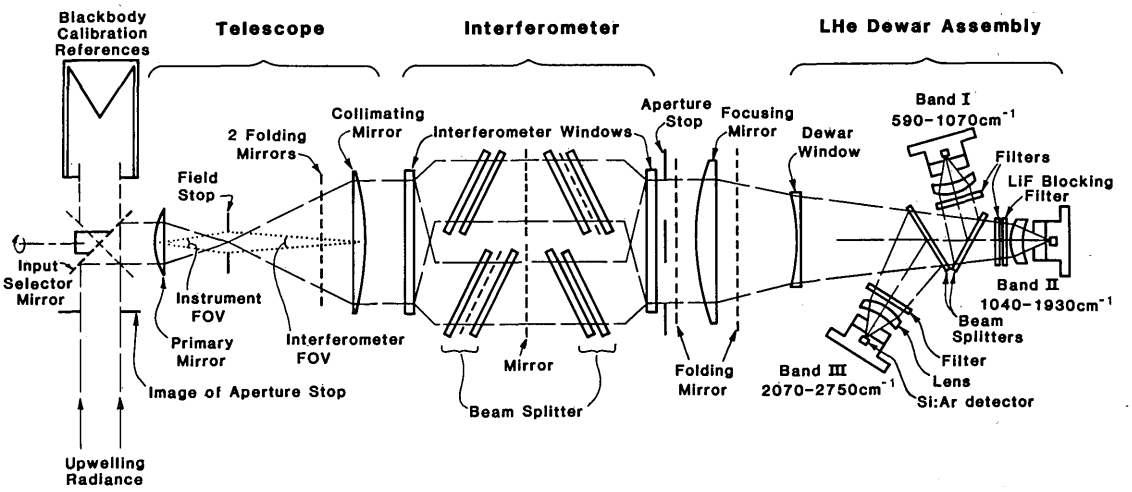

Fig. 1. Functional schematic of HIS optics. The primary mirror, collimating mirror, and focusing mirrors are shown as lenses to simplify the drawing. Plane reflecting surfaces are shown as dashed lines, and the two paths of the interferometer are functionally represented. The complete instrument is ~2.7 m (9 ft) long and fits into the 45.7-cm (18-in.) diam wing pods of the NASA U-2 aircraft.

form has been demonstrated.[9] An aircraft model HIS has been developed and flown on dozens of flights of the NASA U-2 research aircraft as a direct demonstration of the scientific value of such an instrument[10] and that the radiometric noise and calibration requirements are achievable.[11] The instrument was flown with many other atmospheric sensing instruments in two major NASA field programs, the combined Huntsville Meteorological Experiment (COHMEX) for studying severe storms and the First ISCCP Regional Experiment (FIRE) for studying the effect of cirrus clouds on climate. The unique ability of this instrument to measure accurately the emission spectrum from a flexible high-altitude platform with a large complement of other instrumentation should make it an important resource for many types of experiment for several years. Currently, plans for modifying the newest NOAA geosynchronous sounding instrument to incorporate an interferometer are being investigated to realize improvements in the satellite sounding data for weather forecasting before the next century.

This paper describes information about the radiometric calibration of the HIS aircraft instrument, which may be useful to other IR interferometer applications. Early laboratory testing of the aircraft instrument revealed that wavelength-dependent calibration errors of up to 15°C occurred between 600 and 900 cm^{-1} when blackbodies at 300 and 77 K were used to determine the radiance of a 280 K blackbody from the magnitude spectra of each source (Sec. II). These large errors, which were originally believed to require hardware changes to the instrument, have been completely eliminated by the processing technique described in Sec. III. The instrument characteristic responsible for the initial calibration errors is also identified there. The implications of the new calibration analysis technique for interferometer design and performance are summarized in the final section.

II. HIS Radiometric Calibration and the Problem

A. Calibration Approach and Laboratory Test Results

The basic approach for determining absolute radiances from the HIS nadir-viewing interferometer is the same as that used for filter radiometers and has been used successfully for other interferometric applications.[3–7,12] The detectors and electronics are designed to yield an output which is linear in the incident radiance for all wavenumbers in the optical passband of the instrument, and two blackbody reference sources are viewed to determine the slope and offset which define the linear instrument response at each wavenumber.

In the HIS U-2 instrument, calibration observations of the two onboard reference blackbodies are made every 2 min. There are four double-sided optical-path scans of each reference source for every twelve scans of the earth. As shown in Fig. 1, which summarizes the optical configuration, the blackbodies are viewed by rotating the telescope field of view (FOV) from below the aircraft to inside a blackbody aperture using a 45° plane mirror. There are no uncalibrated optical surfaces, since the earth is viewed through an open aperture in the pod, which provides an aerodynamic shell.

The small size of the optical beam at the blackbody positions makes the design of accurate radiation standards relatively easy. The reference blackbodies are thermoelectrically controlled blackened copper cavities. The insulated copper walls of the blackbody cavities give good temperature uniformity, and because of the cavity effect, the normal emissivity is very close to one (Table I). The temperatures are sensed with accurately calibrated platinum resistance thermometers (PRTs) embedded in the base of each cavity. (During testing, a second PRT in the side of the cavity was used to verify adequate temperature uniformity.)

Table I. Characteristics of the HIS Aircraft Instrument

Spectral range (cm^{-1})[a]	
Band I	590–1070
Band II	1040–1930
Band III	2070–2750
Field of view diameter (mrad)	
Telescope	100
Interferometer	30
Blackbody reference sources	
Emissivity	>0.998
Aperture diameter (cm)	1.5
Temperature stability (K)	±0.1
Temperatures (K)	240, 300
Autoaligned interferometer:	Modified BOMEM BBDA2.1
Beam splitter	
Substrate	KCl
Coatings (¼ λ at 3.3 μm)	Ge + Sb_2S_3
Maximum delay (double-sided current configuration (cm)	
Band I (hardware limit is ±2.0)	±1.8
Bands II and III (limited by data system)	+1.2, −0.8
Michelson mirror optical scan rate (cm/s)	0.6–1.0
Aperture stop (at interferometer exit window)	
Diameter (cm)	4.1
Central obscuration area fraction	0.17
Area (cm^2)	10.8
Area-solid angle product (cm^2 sr)	0.0076
Detectors	
Type	Ar-doped Si
Diameter (cm)	0.16
Temperature (K)	6
Nominal instrument temperature (K)	260

[a] The ranges shown are design ranges. The current bandpass filters were chosen from available stock filters and will be changed as new filters are acquired.

One important additional requirement when applying a two-point calibration with blackbody references to an interferometer, as opposed to an instrument measuring spectra directly, is that the instrument responsivity should be independent of optical delay (or that any delay dependences should be accurately known). Avoiding sources of delay-dependent response was a major objective in designing the HIS instrument. To accomplish this, care was taken in the optical stop design and alignment to prevent the effective aperture stop size from changing with the motion of the Michelson mirror. The best location for the aperture stop, which is focused on the detectors, was found to be at the exit window of the interferometer module (see Fig. 1). Furthermore, the FOV of the interferometer is restricted to 30 mrad to limit self-apodization.

Now we turn to the mathematical expressions for the calibration. First, a formalism which leads to the use of magnitude spectra in the expression for calibrated radiance is presented to show where this commonly used approach can create a problem, as occurred with the early (1985) HIS calibrations. Assuming linearity as expressed above, the output interferogram F can be expressed in terms of the incident spectral radiance L_ν as follows, using a continuous representation:

$$F(x) = \frac{1}{2}\int_{-\infty}^{\infty} C_\nu \exp[i\phi(\nu)] \exp(i2\pi\nu x)d\nu, \quad (1)$$

where the uncalibrated magnitude spectrum ($C_\nu \equiv C_{-\nu}$) is given by

$$C_\nu = |\tilde{F}| = r_\nu(L_\nu + L_\nu^0), \quad (2)$$

and where x = optical path difference (delay),
ν = wavenumber,
$\phi(\nu)$ = phase response of instrument [$\phi(\nu) = \phi(-\nu)$],
r_ν = responsivity of instrument,
L_ν^0 = offset from instrument emission, referred to input,
$\sim$ = complex Fourier transform.

The phase characterizes the combined optical and electrical dispersion of the instrument and here is assumed to be the same for scene and background emissions. Although this assumption is commonly made, it will later be shown to be invalid for the HIS instrument. Equation (2) expresses the linear relationship between the uncalibrated spectrum and spectral radiance. The two unknowns to be determined from the two calibration observations are the responsivity and the offset radiance. The offset radiance defined here is the radiance, which, if introduced at the input of the instrument, would give the same contribution as the actual emission from various parts of the optical train. Equation (2) written for both the hot and cold blackbody views can be solved to yield

$$r_\nu = (C_{h\nu} - C_{c\nu})/[B_\nu(T_h) - B_\nu(T_c)], \quad (3)$$

$$L_\nu^0 = C_{h\nu}/r_\nu - B_\nu(T_h) = C_{c\nu}/r_\nu - B_\nu(T_c), \quad (4)$$

where B_ν is the Planck blackbody radiance, and subscripts h and c label the quantities associated with the hot and cold blackbody. [Note that for simplicity the blackbodies are assumed to have unit emittance here. To account for actual emittances ϵ, the Planck radiances should be replaced with $\epsilon B + (1 - \epsilon)B(T_a)$, where T_a is the ambient temperature.] Solving Eq. (2) for the source radiance and substituting from Eqs. (3) and (4) yield the basic calibration relationships:

$$L_\nu = C_\nu/r_\nu - L_\nu^0; \quad (5)$$

$$L_\nu = [(C_\nu - C_{c\nu})/(C_{h\nu} - C_{c\nu})][B_\nu(T_h) - B_\nu(T_c)] + B_\nu(T_c). \quad (6)$$

The ground calibration tests to be reported here consisted of measuring the radiance from a blackbody at ~280 K using calibration blackbodies at 300 and 77 K. The uncalibrated spectra are shown for two of the three HIS spectral bands in Figs. 2 and 3 (see Table I for the nominal spectral coverage of each band). These bands were chosen because band I displays the problem to be discussed here, and band II does not. (Band III also does not.) Both the magnitude and phase are determined directly from a complex Fourier transformation of the measured two-sided interferogram. As will be explained further in Sec. III, the

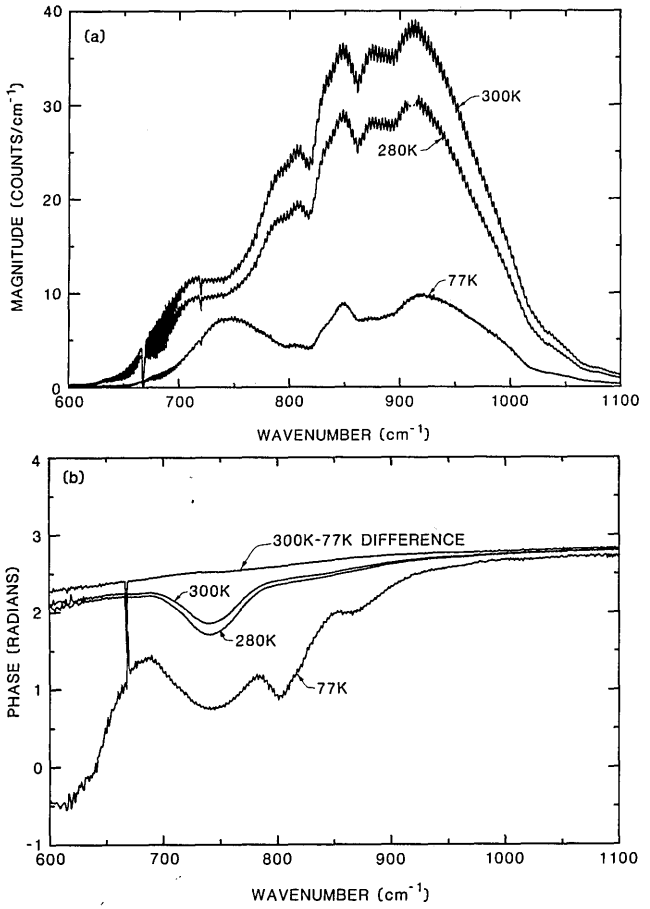

Fig. 2. Uncalibrated magnitude (a) and phase (b) spectra of blackbody sources for HIS spectral band I. The curves are labeled by the temperature of the source. The phase labeled 300K–77K Difference is the phase of the difference of the 300 and the 77 K spectra. The magnitude spectra are shaped by a Gaussian numerical filter and display CO_2 absorption features and channeling as discussed in the text. Note the substantial differences among the phase responses.

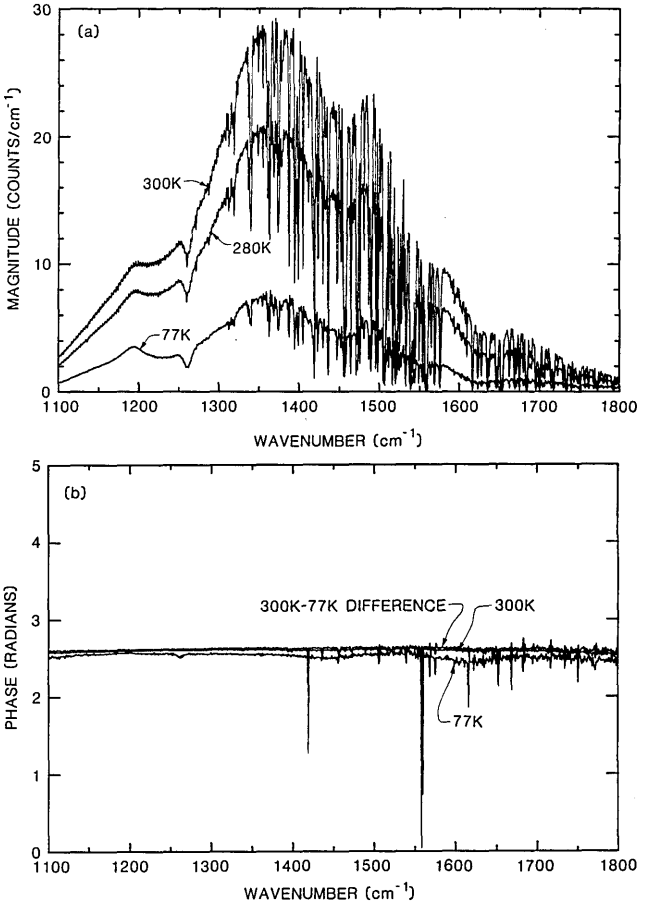

Fig. 3. Uncalibrated magnitude (a) and phase (b) spectra of blackbody sources for HIS spectral band II. The curves are labeled as in Fig. 2. Here also the magnitude spectra are shaped by a numerical filter and display channeling as discussed in the text. The very deep and numerous lines in the magnitude spectra are due to H_2O absorption. In contrast to band I, the phase spectra are very similar and quite linear.

linear phase contribution arising from an ambiguity in the sample offset from the zero path difference (ZPD) has also been removed.

The magnitude spectra have various features which need explanation. Because testing was conducted in air, the instrument transmittance is significantly affected by the 1–2 m of air in the path from the blackbodies to the detectors. (Of the total optical path between the blackbodies and the detector/Dewar assembly, only the interferometer itself is enclosed and backfilled with dry nitrogen to protect the beam splitter; at flight altitudes of 20 km, atmospheric absorption is insignificant.) Therefore, the magnitude spectrum for band I (600–1100 cm^{-1}) shows CO_2 absorption between 600 and 750 cm^{-1}, and band II (1100–1800 cm^{-1}) shows water vapor absorption beyond 1300 cm^{-1}. The absorption for the 668-cm^{-1} CO_2 line and for several H_2O lines is so strong in air that the signal is almost zero, and the phase is poorly defined. The general Gaussian shape of the magnitude spectra is caused by the numerical filtering which is performed in the instrument digital electronics. (A hardware convolution is performed for signal-to-noise preserving sample volume reduction by factors of 14, 8, and 8 in the three spectral bands.)

The sinusoidal components superimposed on the magnitude spectra are channeled spectra caused by the parallel surfaces of the arsenic-doped silicon detectors. (The band III detector has an antireflective coating, and the spectra do not display channeling.) The channeled spectra are very stable because the detectors, which are operated in a liquid He Dewar, have a very small coefficient of expansion and experience only small temperature variations. As will be shown in the next section, channeling does not affect calibrated spectra.

The phase spectra for bands I and II differ markedly. For band II the phases are nearly linear, the behavior expected with an ideal beam splitter having zero dispersion and with an electrical response having a pure time delay. Band I phases, on the other hand, show significant deviations from linearity and also vary as the source radiance is varied. The nonlinearity is optical, not electrical, in origin because the sign of the

deviations from linearity depends on delay scan direction. The phase spectra shown are for one scan direction. The corresponding phases for the other direction are approximately a mirror image about π rad.

B. Problem

It is probably not surprising, in light of the anomalous band I phases, that direct application of the normal calibration procedure (based on magnitude spectra) to the laboratory test data does not work uniformly well. The band I spectrum derived in this way is shown in Fig. 4. The spectrum is presented as a brightness temperature to make any errors stand out as a deviation from the measured blackbody temperature of 280.2 K. Errors of tens of degrees occur, and the similarity of the wavelength dependence of the errors to the nonlinearities of the phase is apparent. Figure 5 shows that the calibrated spectra for the HIS bands with nearly linear phase spectra are extremely accurate when calibrated in the same way. The region of large variance from 280.2 K beyond 1400 cm^{-1} for band II and centered near 2350 cm^{-1} for band III is caused by water vapor and CO_2 in the optical path and does not occur when the instrument is operated at flight altitude. Apparently, the normal calibration approach cannot handle measurements with phase anomalies like those of band I.

III. Solution

A. New Calibration Analysis

The band I phase spectra shown in Fig. 2(b) indicate that the phase becomes more nearly linear as the source radiance becomes larger. This behavior suggests that the total measured interferogram and the corresponding complex spectrum have two components; a normal phase component for radiance from the source and an anomalous phase component for radiance from the instrument itself. Of course, the radiance from the instrument can originate from many individual components with different phase characteristics, but they can be lumped together into one term with one phase.

The new calibration analysis is a generalization which properly accounts for a dual phase response, if it is present. It is really a minor modification of the procedure presented in Sec. II. The difference is that the complete complex spectra obtained from Fourier transforming the measured interferograms are used for calibration, not just the magnitudes. Let the complex uncalibrated spectrum be represented by

$$C'_\nu = \tilde{F}_\nu = r_\nu\{L_\nu + L^0_\nu \exp[i\phi^0(\nu)]\} \exp[i\phi(\nu)], \quad (7)$$

where ϕ^0 is the difference from the normal phase of the anomalous phase associated with the combined radiance from the many emitting components of the instrument. Then it is clear, under the same instrument stability assumptions on which the basic calibration approach depends, that the anomalous phase contribution can be eliminated along with the instrument radiance offset by differencing complex spectra from

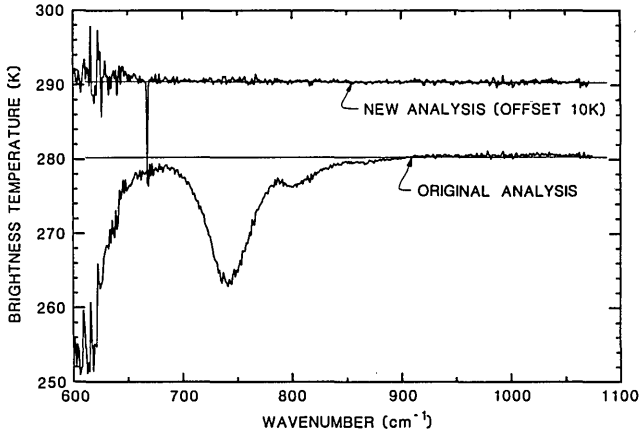

Fig. 4. Brightness temperature spectra for band I. The spectrum with the large deviations from the measured 280.2 K temperature of the blackbody source is derived from the original calibration analysis using magnitude spectra. The spectrum which accurately reproduces a constant brightness temperature is from the modified analysis presented here. The large variance between 600 and 650 cm^{-1} is caused by the low instrument transmittance in that region. Changes have since been made to improve the throughput in this region.

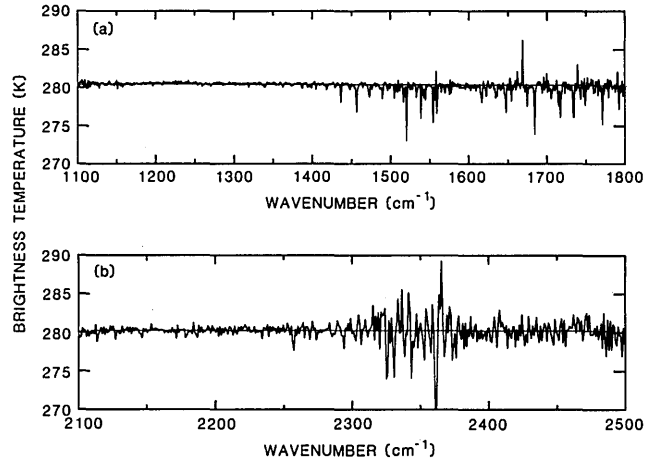

Fig. 5. Brightness temperature spectra for band II (a) and band III (b). The calibration for these bands is good and essentially identical for the standard and modified analyses. The larger variance beyond 1400 cm^{-1} for band II and centered at 2350 cm^{-1} for band III are due to H_2O and CO_2 in the path of the interferometer.

different sources. The difference spectra are identical to the difference spectra which would result if there were no anomalous phase contribution. The equations for the difference spectra from Eq. (7) are

$$C'_\nu - C'_{c\nu} = r_\nu[L_\nu - B_\nu(T_c)] \exp[i\phi(\nu)], \quad (8)$$

$$C'_{h\nu} - C'_{c\nu} = r_\nu[B_\nu(T_h) - B_\nu(T_c)] \exp[i\phi(\nu)]. \quad (9)$$

The new expression for the responsivity, which follows immediately from Eq. (9) by taking the magnitude of both sides, is

$$r_\nu = |C'_{h\nu} - C'_{c\nu}|/[B_\nu(T_h) - B_\nu(T_c)]. \quad (10)$$

Compared to Eq. (3), the difference of magnitude spec-

tra is replaced by the magnitude of difference spectra. The offset which follows directly by substituting the responsivity into Eq. (7) is

$$L_\nu^0 \exp[i\phi(\nu)] = C'_{h\nu} \exp[-i\phi(\nu)]/r_\nu - B_\nu(T_c). \quad (11)$$

Note that while the instrument responsivity remains a real function in this formalism, the offset is now complex. Finally, the basic calibration expression which follows by taking the ratio of Eq. (8) to (9) is

$$L_\nu = \mathrm{Re}[(C_\nu - C_{c\nu})/(C_{h\nu} - C_{c\nu})][B_\nu(T_h) - B_\nu(T_c)] + B_\nu(T_c). \quad (12)$$

For ideal spectra with no noise, this expression for the calibrated radiance would be real, since the phases of the ratioed difference spectra are the same. This cancellation of the phases avoids the square root of two noise amplification, which can be associated with taking the magnitude of spectra with nonzero phase. Because the phase of the ratio of difference spectra is zero to within the noise, the calibrated spectrum can equally well be defined in terms of the real part of the ratio (as shown) or in terms of the magnitude of the ratio.

This technique solves the problem. Application to the measurements presented in the last section yields an accurately calibrated spectrum for band I. The new brightness temperature spectrum, compared to the old in Fig. 4, shows no sign of the large dip centered at 740 cm^{-1}. Also, the phase associated with radiance from the source (the phase of difference spectra) is found to be reasonably linear as shown in Fig. 2. The impact on the band II and III spectra for a 280 K blackbody is negligible. However, the small phase dependence on source for band II would probably cause a detectable error for colder sources.

It should be pointed out that ambiguities in the phase from one spectrum to the next must be eliminated before applying this technique. For the HIS instrument, which does not use a white light source to maintain a fixed offset between ZPD and the delay of a numerically filtered point, a discrete ambiguity occurs. This translational ambiguity is linear in wavenumber and takes the form

$$\phi_k = \pi mk/MR, \quad (13)$$

where k is an integer, m is the spectral sample number, M is the number of points in the spectrum, and R is the numerical filter sample reduction factor. The ambiguity is removed by determining the k for each spectrum, which nearly eliminates the phase slope. Ambiguities of π rad, which occur in instruments with ambient temperature detectors, are not usually a consideration for the HIS application which uses LHe cooled detectors.

Also, note that if a white light source is used to control numerical filtering so that the same delays are measured on subsequent scans, the differencing to eliminate instrument background can be performed on the interferograms. Then anomalous phases would have no effect on spectra. Differencing interferograms is also the way to handle a potential dual phase problem, if one-sided OPD scanning is used.

B. Source of the Anomalous Phase Spectrum

It is of interest to explore the cause of the anomalous band I phase to assess the applicability of the new analysis technique to other FTIR applications. Also, it may be possible to relax constraints on interferometer optical design, since some apparent hardware problems can be eliminated by analysis.

Phase nonlinearities can of course occur from dispersion in beam splitter/compensator substrates, if their thicknesses are not well matched. This effect cannot explain the HIS data. The linearity of the phases for bands II and III suggests that the beam splitter/compensator matching is quite good. More important, dispersion from this origin does not give phase spectra which depend on the source.

To explain the HIS data, a mechanism is needed for which radiance from the instrument can yield a phase spectrum which is different from that for an external source. Apparently, the plane of wavefront division in the beam splitter depends on the source of the radiation. We have identified two mechanisms by which a source dependence might occur: (1) dependence of the beam splitter coating properties on the angle of incidence and (2) emission from the beam splitter coatings.

The first mechanism, angle dependence, has been ruled out as an important factor for the HIS configuration. A test was performed to measure off-axis radiation. It consisted of viewing a LN_2 source with the instrument in its normal configuration and with the field stop removed. The spectrum with the field stop removed is dominated by radiance from the Dewar window entering the interferometer exit window, not radiance from the field stop as in the normal configuration. The difference in the spectra for these two configurations is the spectrum of radiation from the field stop. The phase of the difference is essentially identical to that of radiance from an external source (Fig. 2), indicating no significant dependence on the angle of incidence.

The second possible mechanism, beam splitter coating emission, appears to be a likely candidate for explaining the anomalous phase. Beam splitter emission could lead to the effective wavefront division occurring at the point of emission with coherent radiation being emitted into both legs of the interferometer. Emission at a different depth in the beam splitter than normal wavefront division would create an anomalous phase.

There is evidence that the HIS beam splitter has absorption in the wavenumber region where phases are anomalous. Although the absorption of the beam splitter used for the measurements presented here has not been measured directly, transmittance measurements for other beam splitters of the same construction are available. Figure 6 shows the transmittance of one such beam splitter compared to a sinusoidal fit used to extrapolate the expected transmittance in the absence of absorption into the region of the narrow absorption feature centered at ~740 cm^{-1}. The minimum reflectance at 3000 cm^{-1} is consistent with the

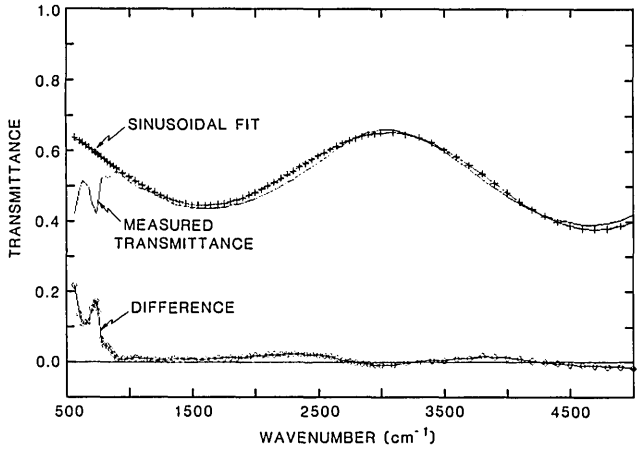

Fig. 6. Transmittance of a beam splitter of the same construction as the HIS instrument beam splitter. The absorption feature centered at ~740 cm^{-1} is responsible for the dual phase response of the instrument. The sinusoidal fit to the transmittance is used to approximate the reflectance for beam splitter emittance and efficiency calculations.

thickness of the beam splitter coatings, 0.25 wavelength at 3.3 μm of Ge and the same of Sb_2S_3. While germanium has a weak absorption feature centered near 740 cm^{-1}, the absorptance of up to 0.1 or 0.2 implied by these data is surprising, because the thickness of the coatings is not large enough for substantial bulk absorption. Maybe the indicated absorption is caused by a surface effect or contamination.

It is possible to obtain information on the beam splitter emittance and efficiency directly from measurements of the HIS instrument itself, if a model of the beam splitter is assumed. The two simple models illustrated in Fig. 7 have been used for this purpose. Rays illustrating the reflection process for an external source and the emission process are shown for both. Model 1 represents the beam splitter/compensator as a single plane with nonzero reflectance ρ and emittance ϵ. It is too simple to explain a phase anomaly, because there is a single surface for wavefront division due to both reflection and emission. Model 2 uses two plane surfaces, one which can reflect but not emit and one which can emit but not reflect. A beam splitter representable by this model would create an anomalous phase.

Emittances and efficiencies are determined from the ratio of the uncalibrated magnitude spectrum for emission from the beam splitter (referred to interferometer input) to that of a blackbody at the same temperature. The blackbody spectrum, free of emission contributions, is obtained in the normal manner by differencing the complex spectrum of an ambient temperature blackbody from the spectrum of a liquid nitrogen blackbody. The beam splitter spectrum is obtained by subtracting a scaled blackbody spectrum from the liquid nitrogen spectrum with the scale factor chosen to give approximately zero from 950 to 1100 cm^{-1} where absorption is expected to be small. The ratio defined in this way is equal to the ratio of the expressions for the emitted and reflected output given

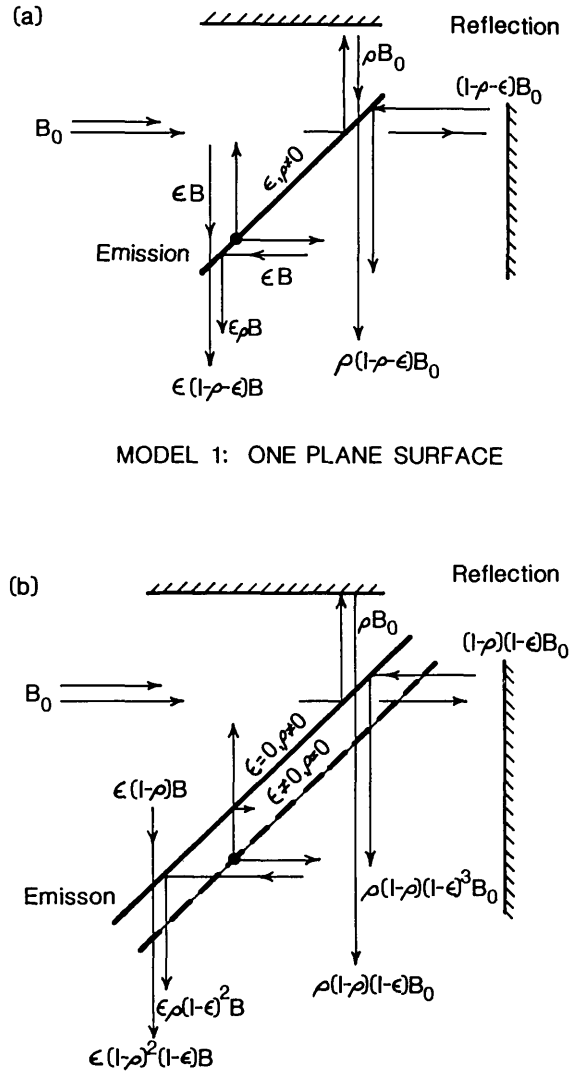

Fig. 7. Simplified beam splitter models for emittance and efficiency calculations. The expressions in terms of the emittance ϵ and reflectance ρ represent the amplitudes of the beam at various locations. The rays on the left represent the emission process, and those on the right represent the passage of an external beam.

in Fig. 7 (e.g., ratio = ϵ/ρ for model 1). Using the reflectivity from the sinusoidal fit of Fig. 6 [fit = $(1-\rho)$], the expression for the ratio can be solved for the emittance. The efficiency of the beam splitter is then given by the product of the complete beam splitter reflectivity and transmittance divided by the ideal output amplitude of 0.25 for a reflectance of 0.5 and no absorptance.

The emittances and efficiencies deduced from interferometer measurements using these models are shown in Fig. 8. The emittances estimates are in reasonable agreement with those obtained from the direct transmittance data of Fig. 6, giving further support for the conclusion that there is beam splitter emission acting approximately as modeled. Notice

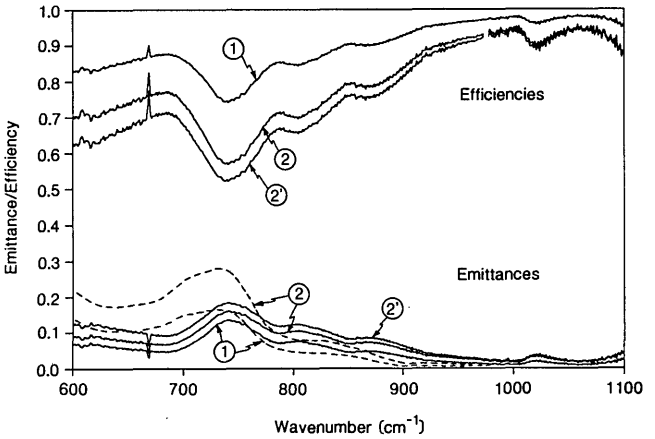

Fig. 8. Beam splitter emittance and efficiency estimates labeled by the model assumed. Model 2′ is the same as model 2 with the emitting and reflecting surfaces reversed in order. The dashed emittance curves are from the data of Fig. 6, and the solid curves are from measurements with the HIS instrument.

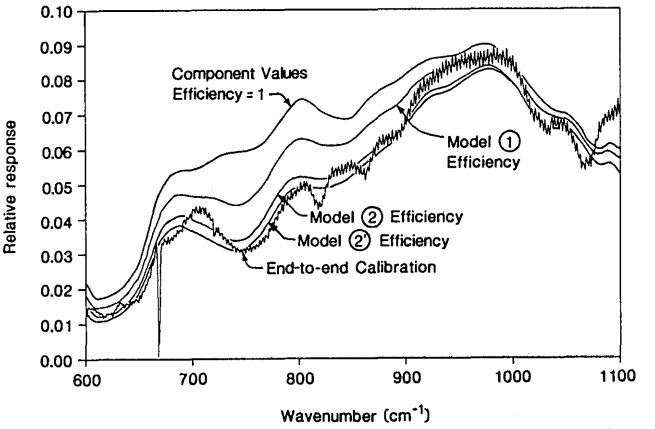

Fig. 9. Comparison of instrument responsivity calculated from optical component transmittances and detector responsivity to the end-to-end responsivity from calibration measurements. The beam splitter efficiencies used in the calculated responsivities are those deduced from measurements with the HIS interferometer itself. The calculations using model 2 seem to account properly for actual beam splitter efficiencies.

that due to the multiple passes through the absorbing layer, the efficiency can get as low as 50% at 740 cm^{-1}.

Further verification of the influence of beam splitter absorption on the HIS instrument is provided by comparison of the measured instrument responsivity to that calculated based on the transmittance of each optical element and on the detector responsivities, as shown in Fig. 9. The Gaussian numerical filter function has been divided out of the measured responsivity (note the effects of CO_2 absorption and channeling discussed earlier). The responsivity calculated assuming the beam splitter to be uniformly efficient is noticeably too large between 650 and 900 cm^{-1} where the band I phase anomaly occurs. The beam splitter efficiencies from Fig. 8 reduce the responsivity over the correct wavenumber region, with the model 2 calculation giving very good agreement with the measured responsivity.

Both the deduced emittances and the efficiencies give a strong case for the emission explanation of anomalous phases. However, a piece of puzzle that does not fit very well is the size of the phase anomalies. The optical thickness ($x = \delta\phi/2\pi\nu$) corresponding to the observed phase anomalies ($\delta\phi$) at 740 cm^{-1} is 3.9 μm. Model 2 suggests that, if the absorption is in the coatings, the additional optical path difference should be <1.9 μm, the optical thickness of the combined beam splitter coatings divided by the cosine of the 30° angle of incidence. This peculiarity and the mechanism for the absorption are remaining mysteries.

IV. Implications and Summary

It is not known whether the problem identified here is common or rare in other FTIR applications. The errors resulting from this problem could possibly be small enough to go unnoticed but might be significant when evaluating detailed performance. Comparing the phase spectra for a cold and a warm source is a simple test for diagnosing the problem.

The new calibration analysis technique has been discussed here in the context of the HIS application, involving absolute radiance measurements. It may also be important for applications in which the transmittance or reflectance of a sample is measured. As pointed out by Tanner and McCall,[13] emission from the samples or the surroundings can create significant errors for these types of measurement. However, the radiance contribution from the background can be eliminated, if the spectra for two different reference sources are differenced. By determining the difference spectra using complete complex spectra as described in the last section, any anomalous phase contributions of radiance from the interferometer will also be eliminated.

There are some aspects of interferometer design that may be influenced by the analysis approach presented here and by knowledge that beam splitter emission can modify the phase response. First, the constraints on beam splitter coating materials can probably be relaxed to include materials with some absorption. Second, interferometer designs may be able to rely on a better capability to handle errors associated with the phase. It is conceivable that having a well-behaved phase is not so important when a proper calibration is performed with double-sided scanning.

In summary, the phase response of one spectral band of the HIS FTIR instrument appears to vary with the source radiance, becoming more linear the higher the radiance contribution from the source. This dependence creates substantial radiance errors when magnitude spectra are used to perform a two-point calibration using blackbody reference sources. The errors are eliminated, yielding good calibration results, when a minor modification to this technique is applied. The new technique explicitly accounts for the possibility that a dual phase response can occur. That is, the phase response for radiance from the instrument can

differ from that for radiance from a source. The origin of the different phase response for radiance from the HIS instrument is identified as emission from the beam splitter.

The authors thank the members of the instrument team at the Space Science and Engineering Center, BOMEM, Inc., the Santa Barbara Research Center, and the University of Denver, whose care in fabricating and aligning the HIS instrument made accurate radiometric calibration realizable. Thanks also to Frank Murcray for many helpful discussions. The HIS program is jointly funded by NOAA contract NA-84-DGC-00095 and NASA contract NAS5-27608.

References

1. W. L. Smith, H. E. Revercomb, H. B. Howell, and H. M. Woolf, "Recent Advances in Satellite Remote Sounding," *International Radiation Symposium '84: Current Problems in Atmospheric Radiation*, G. Fiocco, Ed. (A. Deepak, Hampton, VA, 1984), p. 388.
2. W. L. Smith, H. E. Revercomb, H. B. Howell, and H. M. Woolf, "HIS—A Satellite Instrument to Observe Temperature and Moisture Profiles with High Vertical Resolution," in *Fifth Conference on Atmospheric Radiation* (American Meteorological Society, Boston, 1983).
3. R. A. Hanel, B. Schlachman, F. D. Clark, C. H. Prokesh, J. B. Taylor, W. M. Wilson, and L. Chaney, "The Nimbus III Michelson Interferometer," Appl. Opt. **9**, 1767 (1970).
4. R. A. Hanel, B. Schlachman, D. Rodgers, and D. Vanous, "Nimbus 4 Michelson Interferometer," Appl. Opt. **10**, 1376 (1971).
5. D. Oertel *et al.*, "Infrared Spectrometry of Venus from Venera-15 and Venera-16," Adv. Space Res. **5**, 25 (1985).
6. R. A. Hanel *et al.*, "Mariner 9 Michelson Interferometer," Appl. Opt. **11**, 2625 (1972).
7. R. A. Hanel *et al.*, "Infrared Spectrometer for Voyager," Appl. Opt. **19**, 1391 (1980).
8. J. W. Brault, "Fourier Transform Spectroscopy," *High Resolution Astronomy*, Proceedings, Fifteenth Advanced Course in Astronomy and Astrophysics, Saas-Fee, M. Huber, A. Benz, and M. Mayor, Eds. (1985).
9. "A Design Feasibility Study for the High-Resolution Interferometer Sounder (HIS)," Santa Barbara Center Final Report for contract UAA 871R55 5 (10 July 1981, updated 19 July 1982, updated 15 Feb. 1983).
10. W. L. Smith, H. E. Revercomb, H. M. Woolf, H. B. Howell, D. D. LaPorte, and K. Kageyama, "Improved Geostationary Satellite Soundings for the Mesoscale Weather Analysis/Forecast Operations," in *Proceedings, Symposium on Mesoscale Analysis and Forecasting*, Vancouver, Canada, 17–19 Aug. 1987, ESA SP-282 (1987).
11. H. E. Revercomb, D. D. LaPorte, W. L. Smith, H. Buijs, D. G. Murcray, F. J. Murcray, and L. A. Sromovsky, "High-Altitude Aircraft Measurements of Upwelling IR Radiance: Prelude to FTIR from Geosynchronous Satellite," Mikrochim. Acta in press, 000 (Springer-Verlag, Wien, 1987).
12. D. D. LaPorte and R. Howitt, "Ambient Temperature Absolute Radiometry using Fourier Transform Spectrometers," Proc. Soc. Photo-Opt. Instrum. Eng. **364** (1982).
13. D. B. Tanner and R. P. McCall, "Source of a Problem with Fourier Transform Spectroscopy," Appl. Opt. **23**, 2363 (1984).

Meetings *continued from page 3123*

1989
February

19–23 **Optical Fiber Communication Conf., Dallas** *OSA Mtgs. Dept., 1816 Jefferson Pl., NW, Wash., DC 20036*

21–24 5th Symp. on Optical Fibers & Their Applications, Warsaw *R. Romaniuk, IPE, Warsaw U. of Tech., Nowowiejska 15/19, PL-00-665 Warsaw, Poland*

26–3 Mar. 1989 Santa Clara Symp. on Microlithography, Santa Clara *SPIE, P.O. Box 10, Bellingham, WA 98227*

27–1 Mar. **Optical Computing Top. Mtg.,** Salt Lake City *OSA Mtgs. Dept., 1816 Jefferson Pl., NW, Wash., DC 20036*

March

1–3 **Photonic Switching II Top. Mtg.,** Salt Lake City *OSA Mtgs. Dept., 1816 Jefferson Pl., NW, Wash., DC 20036*

6–8 **Quantum Wells for Optics & Optoelectronics Top. Mtg.,** Salt Lake City *OSA Mtgs. Sept., 1816 Jefferson Pl., NW, Wash., DC 20036*

8–10 **Picosecond Electronics & Optoelectronics Top. Mtg.,** Salt Lake City *OSA Mtgs. Dept., 1816 Jefferson Pl., NW, Wash., DC 20036*

12–17 Advances in Semiconductors & Superconductors: Physics & Device Applications courses, Bay Point, FL *SPIE, P.O. Box 10, Bellingham, WA 98227*

13–17 Color '89 Mtg., Buenos Aires *Grupo Argentino del Color, c/o Div. Optica, INTI, C.C. 157, 1650 San Martin (BA), Argentina*

22–24 8th Ann. IEEE Int. Phoenix Conf. on Computers & Communications, Scottsdale *A. Pizzarello, Honeywell Bull Inc., P.O. Box 8000, M/S Z-10, Phoenix, AZ 85066*

27–31 1989 Technical Symp. Southeast on Optics, Electro-Optics, & Sensors *SPIE, P.O. Box 10, Bellingham, WA 98227*

April

24–28 **Lasers & Electro-Optics Conf., Baltimore** *OSA Mtgs. Dept., 1816 Jefferson Pl., NW, Wash., DC 20036*

24–28 **Int. Quantum Electronics Conf., Baltimore** *OSA Mtgs. Dept., 1816 Jefferson Pl., NW, Wash., DC 20036*

24–28 2nd Int. Congr. on Optical Sci. & Eng., Paris *SPIE, P.O. Box 10, Bellingham, WA 98227*

30–4 Aug. 33rd Ann. Int. Tech. Symp. on Optical & Opto-Electronic Applied Sci. & Eng., San Francisco *SPIE, P.O. Box 10, Bellingham, WA 98227*

continued on page 3249